Finite element analysis of mechanical behavior, permeability of irregular porous scaffolds and lattice-based porous scaffolds

Article (Accepted Version)

Finite element analysis of mechanical behavior, permeability of irregular porous scaffolds and lattice-based porous scaffolds

To cite this article before publication: Yue Du *et al* 2019 *Mater. Res. Express* in press https://doi.org/10.1088/2053-1591/ab3ac1

Finite element analysis of mechanical behavior, permeability of irregular porous scaffolds and lattice-based porous scaffolds

Yue Du[1, 3, §], Huixin Liang[1, §], Deqiao Xie[1], Ning Mao[1, 4], Jianfeng Zhao[1], Zongjun Tian[1], Changjiang Wang[2], Lida Shen[1, *]

[1]*College of Mechanical and Electrical Engineering, Nanjing University of Aeronautics and Astronautics, 29 Yudao Street, Nanjing 210016, PR China.*

[2]*Department of Engineering and Design, University of Sussex, Sussex House, Brighton BN19RH, United Kingdom.*

[3]*Suzhou Kangli Orthopedics Instrument Co, Ltd, Suzhou, 215600, PR China.*

[4]*Suzhou Yunzhi Medical Technology Co, Ltd, Suzhou, 215600, PR China.*

§These authors contributed equally.

*Correspondence: ldshen@nuaa.edu.cn (L.D. Shen); Tel.: +86-025-84892520

Abstract

In view of the low elastic modulus of the porous structure, it has attracted extensive attention in the field of artificial tissue implants for bone tissue engineering, and it has become important to find a porous structure suitable for human bone tissue.

In this study, we constructed three type regular porous structure (cube, diamond, rhombohedral dodecahedron) and an irregular porous structure based on Voronoi tessellation. Firstly, the structural characteristics of porous structures were studied. After permeation simulation and compression

simulation, we found that the structural characteristics (porosity, pore size, specific surface area) of four porous structures have a strong positive correlation with permeability. With the increase of porosity, the effective elastic modulus of the four porous structures decreases gradually. When the porosity is 80%, the effective elastic modulus and permeability of the four porous structures can basically meet the requirements of human bone implants. Irregular porous scaffolds exhibit relatively limited anisotropy in terms of mechanical properties and permeability. In view of the similarity between the structure and the human bone, the irregular porous structure exhibits superior development and application potential compared to the regular porous structure

Keywords: Porous scaffolds; Finite element analysis; Mechanical behavior; Permeability; Anisotropy

1. Introduction

In recent years, the development of new artificial implants has expanded the field of bone tissue engineering, especially with the development of additive manufacturing technology, which has resulted in porous metal implants with different structures and different materials, which are replacing traditional solid implants. This is because the former can greatly reduce the stress shielding effect and micro-motions caused by the latter [1]. It is said that in more than 70% of cases, aseptic loosening is the main cause of implant failure, an important reason for aseptic loosening is micro-motions and stress shielding [2.3].

The most critical component in bone tissue engineering for orthopedic reconstruction is the scaffold, which serves as a base frame for cell interaction and bone-extracellular matrix to provide support for new tissue formation [4]. In general, an ideal bone scaffold needs to have the following

four basic characteristics: 1. Good biocompatibility, 2. Mechanical properties matched to the transplant site, 3. Interconnected pore network to ensure cell migration and nutrient waste transport, 4. Surface features suitable for cell attachment [5-9]. However, designing an optimal porous structure is a complex process that involves optimizing and balancing the relationship between structural properties (including porosity, pore size, specific surface area) and mechanical properties, biocompatibility, etc.

For mechanical properties, it mainly refers to the modulus of elasticity and the compressive strength. On the one hand, the elastic modulus of the porous structure must match the human bone elastic modulus to alleviate the side effects caused by stress shielding. On the other hand, the bone implants itself must have a certain strength to serve as load-bearing device. Assessing the permeability of the porous structure is critical to the biological activity of the cells within the scaffold. The permeable scaffold should allow for efficient nutrient and gas diffusion as well as waste discharge through its channels. The structural properties (porosity, pore size, specific surface area, etc.) are closely related to mechanical properties and permeability. For example, the classic Gibson-Ashby summarizes the relationship between porosity and mechanical properties [10].

At present, open scaffolds can be roughly divided into unit cells and irregular porous cells. Most of these studies focus on unit cells such as cube [1, 11], diamond [11, 12, 13], rhombic dodecahedron [14, 15], octahedron [16, 17], etc. In the irregular porous unit, the irregular porous structure based on the Voronoi tessellation structure is the most attractive [18, 19]. In many studies, the main focus is on the topology optimization of scaffold, mechanical properties, biocompatibility and other characteristics, especially the comparative study between irregular porous structure and regular porous structure is lacking.

The aim of this study was to investigate the relationship between structural characteristics (porosity, pore size, specific surface area) of regular porous structures and irregular porous structures, as well as their mechanical strength and permeability. To this end, we first constructed three models of regular porous structure (cube, diamond, rhombic dodecahedron) and the models of irregular porous structure, and analyzed their porosity, pore size and specific surface area. The porosity of each model was set to 50%, 60%, 70%, 80% and 90%. Via compression and permeability simulation, the relationships between structural characteristics and mechanical properties, permeability are established.

2. Materials and methods

2.1 Modeling and characterization of porous scaffolds

All models are implemented by the Grasshopper plug-in in Rhino 6 (McNeal, Seattle, WA, USA). The parametric design features of the software allow us to precisely control the structural parameters of the model, and on the other hand allow us to measure the porosity and specific surface area of the model.

Irregular porous structure is based on Voronoi tessellation and stems from our improvement on previous work [19]. First, we arrange a uniform lattice in the cubic space. The distance between adjacent points is d. These points are called original points, using the original points as the center of the sphere, construct a sphere of radius r, where $0<r<0.5d$. Randomly generate a point in each sphere constructed, these random points are called seed points, where the irregularity $i = r / d$. Then a 3D Voronoi diagram based on the seed point is constructed. We extract the 3D Voronoi diagram wireframe and then form a strut of a circle with a cross-sectional diameter D based on these frames.

Then, an irregular porous scaffolds were constructed and its control parameters include strut diameter *D*, unit distance *d*, irregularity *i*, a single Voronoi porous scaffold can be seen in Figure 1(f).

For the regular porous structure, a unit cell frame is first constructed with a side length *d*, and then arrayed in a three-dimensional space, and then based on this, a struts of a circle having a cross-sectional diameter *D* is formed. Such a regular porous structure is constructed, in which the control parameter are strut diameter *D*, unit distance *d* (side length), this can be seen in Figure 1(a), (b), (c).

In order to accurately describe the structural characteristics of porous structures, we analyzed and measured the porosity, pore size and specific surface area with the powerful parametric ability of grasshopper software. For the sake of comparison the regular porous scaffolds and irregular porous scaffolds, in this study, the irregularity of the irregular porous structure was determined to be an intermediate value, that is, i=0.25. And strut diameter *d* of all four porous scaffolds was 0.5mm. The adjustment of the structural characteristics of the four porous structures (porosity, pore size, specific surface area) is completed by adjusting the unit distance *d*. Finally, each of the four porous structures was modeled separately by five porosity gradients 50%, 60%, 70%, 80%. 90%. The basic unit of these four porous structures can be seen in Figure 1. And Figure 2 shows four porous structures with a porosity of 70%.

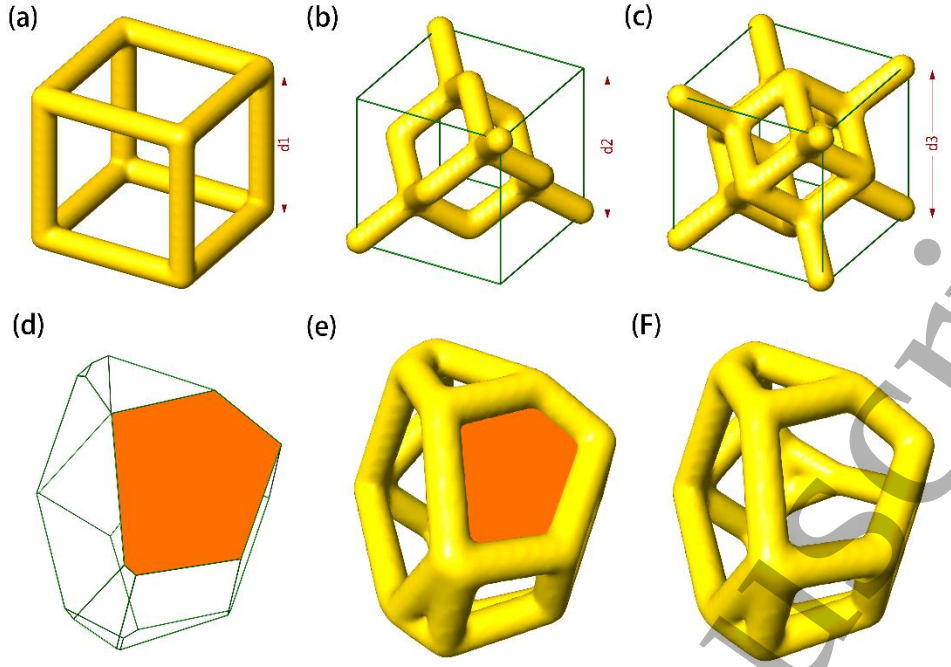

Figure 1. Single cell of the four porous scaffolds. (a) Cube scaffold. (b) Diamond scaffold. (c) Rhombic dodecahedron scaffold. (d) Single irregular porous frame with a pore surface. (e) Single irregular porous scaffold with a pore surface. (f) Single irregular porous scaffold.

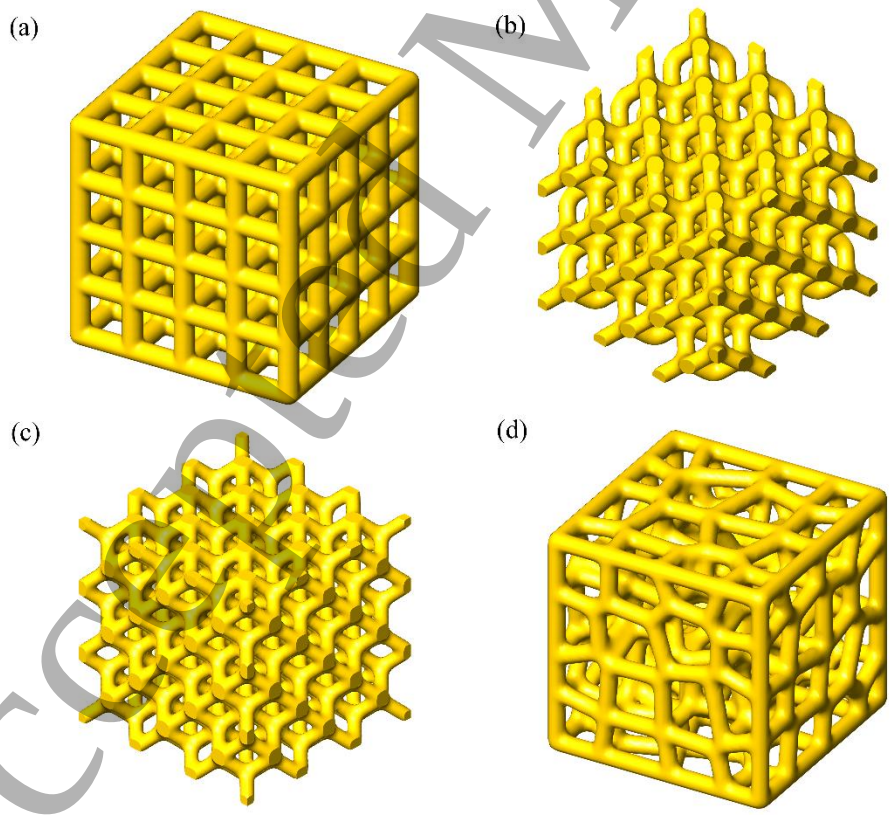

Figure 2. Four porous structures with a porosity of 70%. (a) Cube scaffolds. (b) Diamond scaffolds.

(c) Rhombic dodecahedron scaffolds. (d) Irregular porous scaffolds.

The porosity P of each model is calculated by Eq 1. Especially for Diamond scaffolds and Rhombic dodecahedron scaffolds, the model of the porous structure is obtained by Boolean operation, and Boolean operations will result in a smaller porosity of the porous structure. For example, when the porosity of Diamond scaffolds and Rhombic dodecahedron scaffolds is 70%, the porosity without Boolean operation is 72.13% and 72.21%, respectively. In order to facilitate the simulations, the porosity of Diamond scaffolds and Rhombic dodecahedron scaffolds is the porosity of the model by Boolean operation. As for regular porous scaffolds, Pore size R is defined as the diameter of circle of the same area as the lattice pore face, summarized by the following Eq 2. Particularly, in the diamond structure, because the pore is a space hole and not in a plane, we use the projection to obtain a plane pore, and obtain the area of the pore. In view of the pores size of the irregular porous structure is not uniform, therefore, the pore size of the irregular porous structure in the text refers to the average value of the pore diameter calculated by the formula 3. Figure 1(d) shows single irregular porous frame with a pore surface and figure 1(e) presents single irregular porous scaffold with a pore surface. The specific surface area is defined as the ratio of the area of the porous structure to the volume of the porous structure, drawn by the following Eq 4. Closed pore ratio R^* refers to the ratio of closed pores to total number of pores.

$$P = 1 - V_p/V \quad (1)$$

Where P, V_p, V are porosity, volume of the porous scaffolds, outer volume of the porous scaffolds.

$$R = \sqrt{4S_p/\pi} \quad (2)$$

$$R = \frac{1}{n}\sum_1^n \sqrt{4S_p/\pi} \quad (3)$$

Where R, S_p, n are pore size, lattice pore area and total number of pores.

$$S^* = S/V_p \quad (4)$$

Where S^*, S, V_p are the specific area, area of porous scaffolds, volume of porous scaffolds.

2.2 Fluid flow simulation

The fluid flow simulation domain was obtained in Rhinoceros 6 after Boolean subtraction of the scaffold geometry from the volume-of-interest. These domains were exported in STL format to Comsol Multiphysics (COMSOL Group, Stockholm, Sweden). Modeling and meshing of irregular porous structures is shown in Fig. 3. Computation Fluid Dynamic (CFD) analysis of the scaffolds was approximated by laminar and stationary Navier-Stokes model. The Dulbecco's modified Eagle's medium (DMEM) was modeled as incompressible water with dynamic viscosity of u= 0.00145 Pa s and density of 1000 kg/m^3[20], boundary conditions included an inlet flow of 1mm/s, null outlet pressure, and no-slip conditions. For the regular porous scaffolds, simulations were done only along Z axes direction, but considering anisotropy, for irregular porous supports, the simulation is performed along the X-, Y-, and Z-axes. Permeability K was determined on the basis of Darcy's relationship (Eq. (5)).

$$K = V_D \cdot u \cdot L/\Delta P \quad (5)$$

Where K, V_D, u , L ,$\triangle P$are Permeability coefficient, Darcy velocity, dynamic viscosity, lattice length, pressure gradient across the fluid domain.

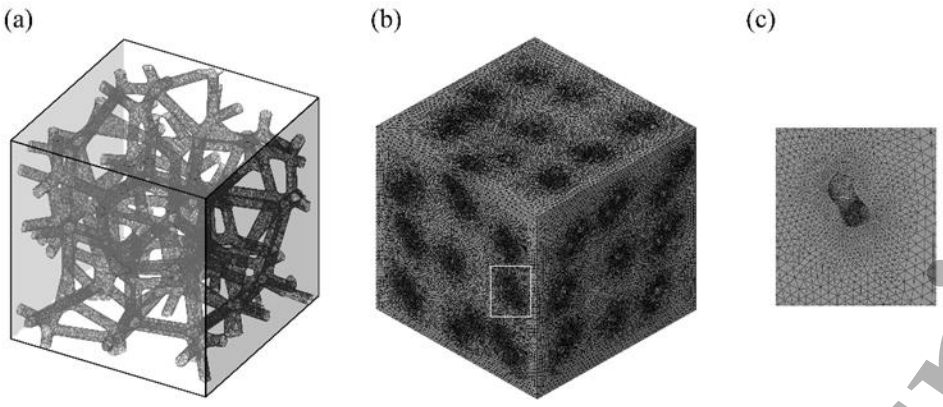

Figure 3. Preparation process of fluid flow simulation. (a) A selected irregular scaffold with a porosity of 70% by Boolean operation. (b) Fluid simulation finite element model of the selected scaffold. (c) A partial mesh magnified view of selected area.

2.3. *Mechanical simulations*

FEA (abaqus 6.14, Dassault System, SIMULIA) was performed for each porous scaffolds. The STL model file obtained by Rhino 6 software first generates surface mesh in 3-matic (Materialise，Belgium) and the surface mesh is transformed to body mesh in Abaqus software. Finally, four-node tetrahedral element (C3D4) were formed, and the element side length for the 3D mesh was set as 0.1 mm for all four porous scaffolds types.

A Finite element model of the porous scaffolds is illustrated in Figure 4. Two rigid plates are attached to the porous structures. The upper plate moves being displaced to an axial strain (compression) of 0.01 and the lower one is fixed by constraining all degrees of freedom. To avoid interpenetration, a frictionless general contact is defined between the porous structure and the rigid plates.

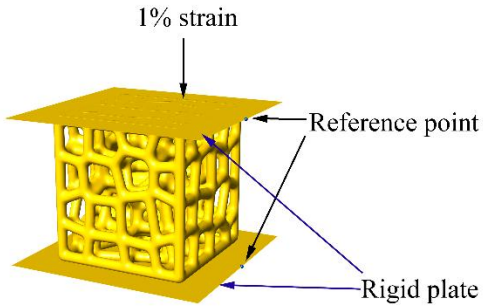

Figure 4. A Finite element model of the irregular porous scaffolds.

In simulation, model properties was set according to Ti6Al4V with the density of 4.41 g/cm^3, the elastic modulus of 110 Gpa and the Poisson's ratio of 0.3[21]. During the simulation process, the analysis steps were dynamic and explicit. For the regular porous scaffold, the simulation was performed only in the Z-axis direction, but the anisotropy was considered for the irregular porous structure, and the simulation was performed along the X-, Y-, and Z-axes. Finally, the maximum Von Mises stress and effective elastic modulus, the average von Mises stress were recorded

3. Results and discussion

3.1 Structrue characteristic of the four porous scaffolds

It can be seen from Fig. 1 that the unit cell of the regular porous structure (cube, diamond, rhombic dodecahedron) has a regular pore shape and an equal pore size. The number of complete pores of the unit cell of the three regular porous structures is 6, 4, and 12, respectively. For a Voronoi cell with an irregular porous structure, there are 15 complete pores, and the shapes and sizes of the pores are all different. In fact, the smaller pores in the irregular porous structure will disappear due to the larger strut diameter. This can also be seen from the Voronoi cell scaffold in Figure 1(e).

Figure 5 shows the pores size distribution of irregular porous structure with porosity of 70%, except for closed pores. It can be seen from Fig. 5(a) that the pore diameter of the 257 through-holes

of the irregular porous structure exhibits a tendency to increase in fluctuation, and as seen from Fig. 5(b), the fluctuation of the pore size distribution is relatively large. Figure 6 shows pores size distribution of the irregular porous structure at five different porosity gradients, here, pores size are divided into four intervals: closed pores (pore size R<0μm); small pores (0<R<200μm); medium pores (200um≤R≤1200μm); large pores (R>1200μm); Previous studies have shown that a suitable pore size for bone cell growth is 200 to 1200μm [22].It can be seen from Figures 5 and 6 that the pores size of the irregular porous structure is scattered and covers a range of pores size suitable for bone cell growth. As the porosity increases, a considerable proportion of large pores will occur. It is worth noting that the pores of the irregular porous structure are spatially scattered, in other words, many large pores are concentrated in a certain region. .In contrast, the regular porous structure pores have the same morphology and size, so when the porosity reaches 90%, the pore sizes of the all four structures exceed 1200μm in the figure 7(a), and the average pore diameter of the irregular porous structure is the lowest value of the four structures (1571μm), and 28.39% of the pores still meet the pore size range (200-1200μm) suitable for bone cell growth. In the specific surface aspect, the larger the specific surface area, the better the cell adhesion. As is presented in Figure 7(b), the specific surface areas of the four porous structures increase with the increase of porosity, but the diamond porous structure has a greater surface area than the other three.

In general, as the porosity increases, the specific surface area of the irregular porous structure is slightly lower than that of the regular porous structure, and the pore growth is relatively gentle and substantially satisfies the ideal size range in which the bone cells are suitable for growth. The scattered distribution of through pores in the space and the scattered distribution of the pore size distribution of the irregular porous structure undoubtedly result in its better imitation of the human

bone structure as compared to the regular porous structure.

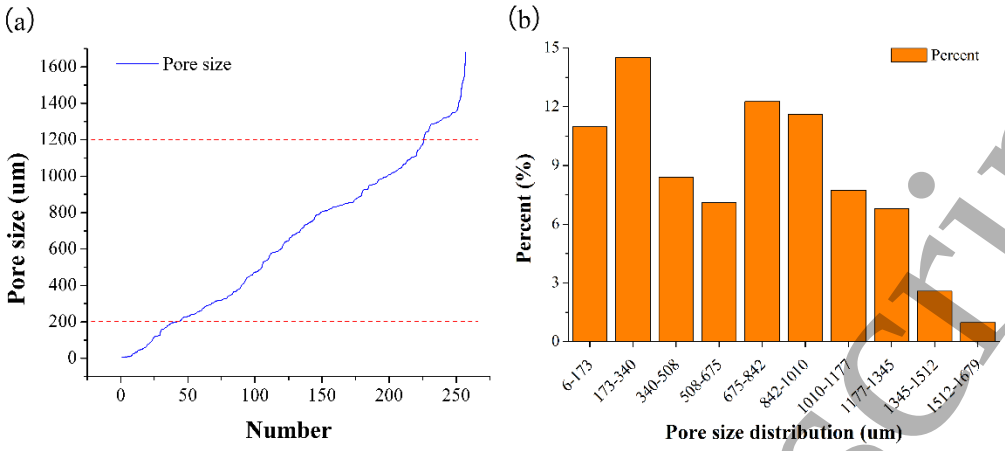

Figure 5. Pore size distribution of irregular porous scaffold with porosity of 70%. (a) Curve graph. (b) Histogram.

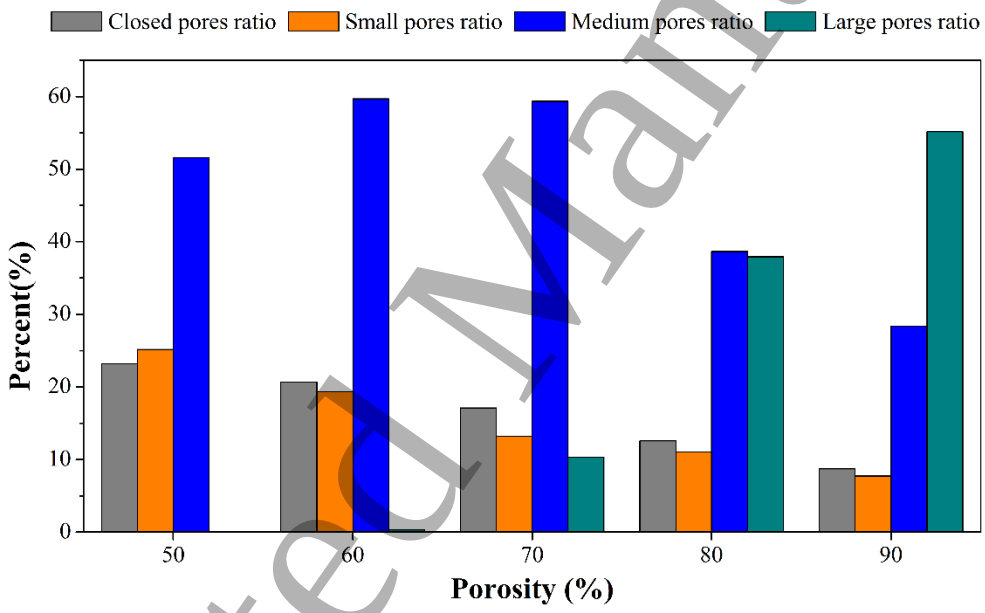

Figure 6. Pore size distribution of the irregular porous structure at five different porosity.

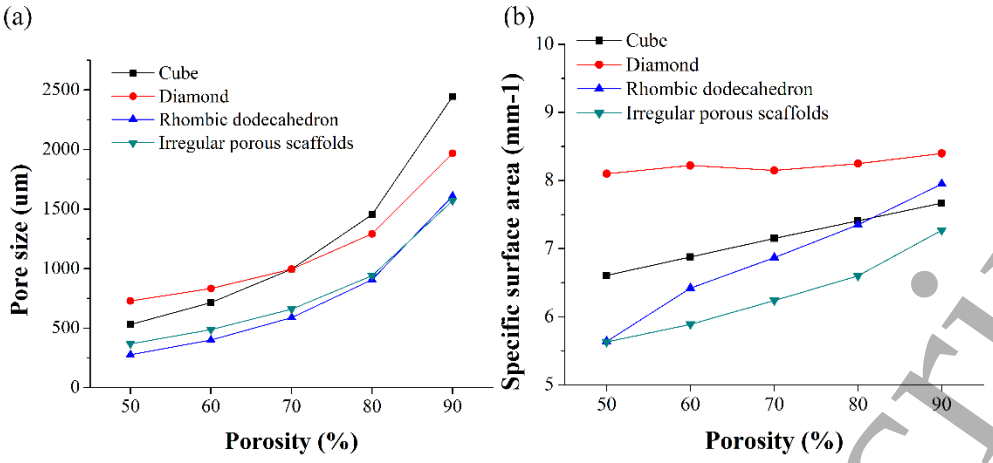

Figure 7. Relation between porosity and (a) pore size, (b) specific surface area.

3.2 Permeability

Figure 8 presents the velocity contour for the four porous structures with 70% porosity obtained by fluid flow simulation. The fluid velocity of the regular porous structure is regularly and evenly distributed. But the fluid velocity distribution of the irregular porous structure is disordered, and the maximum velocity is often concentrated in a partial region. It can be seen from Fig. 9 that the permeability of the irregular porous structure is comparable to that of the three regular porous structures, and when the porosity is greater than 70%, the permeability is greater than that of the regular porous structures.

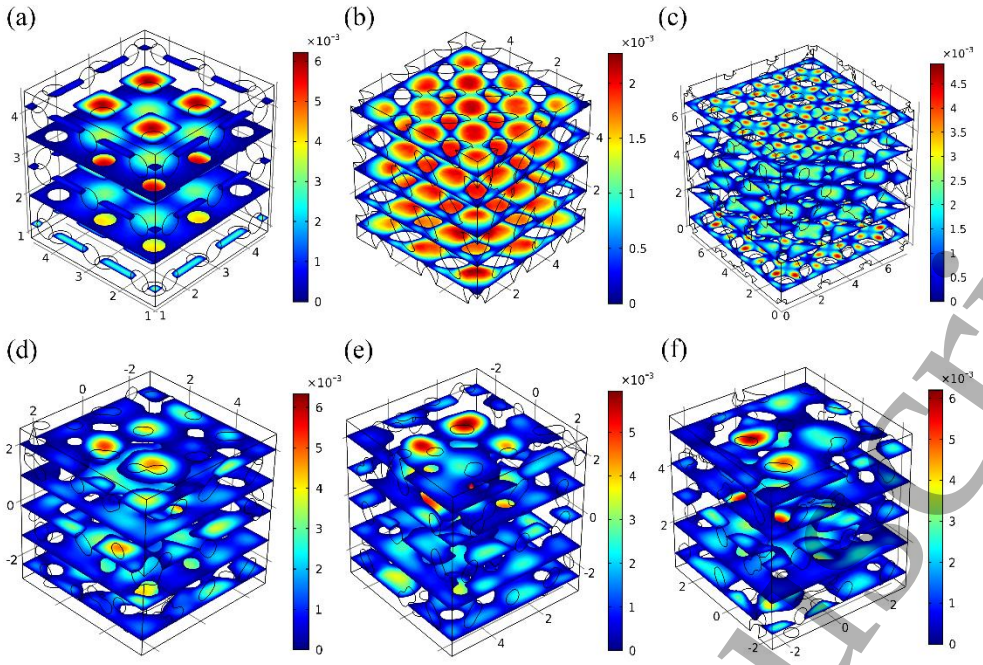

Figure 8. Velocity contour of fluid flow simulation for the four porous scaffolds with 70% porosity. (a) Cube scaffolds. (b) Diamond scaffolds. (c) Rhombic dodecahedron scaffolds. (d-f) Irregular porous structure simulated alone different directions (from left to right: X, Y and Z axis)

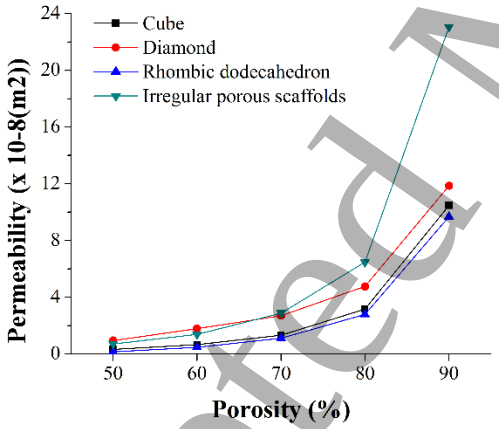

Figure 9. Relation between porosity and permeability of four porous scaffolds.

As can be seen from Figures 7(a), 7(b), and 9, which consider the relationship between porosity and pore size, specific surface area, and permeability, respectively, the permeability of these four types of porous structures increases as the three structural properties (porosity, pore diameter, specific surface area) increase to varying degrees. In terms of permeability, the irregular porous

scaffolds can achieve a larger coverage interval than the other three regular porous scaffolds, and at a porosity of 90%, the permeability reaches the maximum value of the four structures of $23.05 \times 10^{-08} m^2$. It may be related to the pore size distribution of the irregular porous structure. When the porosity reaches 90%, the large pores ratio increases rapidly to 55.16%. Compared with the three types of regular porous structures with a porosity of 90%, the irregular porous scaffolds reached the highest permeability under the condition of the minimum average pore size of 1571μm.

S. Gómez et al constructed irregular porous structure by Voronoi tessellation method. When the porosity is between 40% and 90%, the permeability values ranged from $0.5 < K(x10^{-8}m^2) < 4.5$ [23]. In comparison, the irregular porous structure in this study has a larger range of permeability and better controllability of permeability. Considering that the surface area of the actual porous samples after the additive manufacture will become larger than before and the friction of the liquid flow will also increase, it is therefore necessary for the porous model to have a greater range than the above-mentioned permeability range. The permeability of the four porous structures in Figure 9 is basically consistent with the range of trabecular permeability found in previous experiments [24-26].

Taking into account the special structural characteristics of irregular porous structures, their pores are not only randomly distributed in space, but their pore sizes also exhibit the characteristics of a scattered distribution within a certain range. More importantly, On the one hand, this human bone-like structure has a certain number of large pores distributed in space, which improves the permeability of the irregular porous structure and ensures the flow of oxygen and nutrients. On the other hand, a large number of small pores mean irregular porous structures, it has a large number of areas where the struts are concentrated. These areas have poor permeability and are suitable for cell adhesion and proliferation.

In our previous study, the irregular porous structure was performed by the similar modeling method, thanks to the appropriate pore size distribution characteristics, performed well in osteoblast proliferation and differentiation in vitro experiments [27]. Compared to regular porous structures, and the controllability of the structural design parameters could makes it possible to achieve both of these two aspects by adjusting the pores size distribution in the irregular porous scaffolds.

3.3 Mechanical characterization

Figure 10 shows elastic modulus versus porosity for all four porous models, The elastic modulus of the four porous structures decreased with increasing porosity, and the elastic modulus of rhombic dodecahedron porous scaffolds obtained the maximum coverage from 5.29 to 120.04 Gpa. When the porosity reaches 80% or higher, the elastic modulus of the four porous structures falls within the range (3-30 Gpa) of the human cortical bone elastic modulus [28]. Of course, for the four porous structures, by adjusting the unit distance *d*, the strut diameter *D*, and the irregularity *i*, a larger adjustment range of the effective elastic modulus can be obtained.

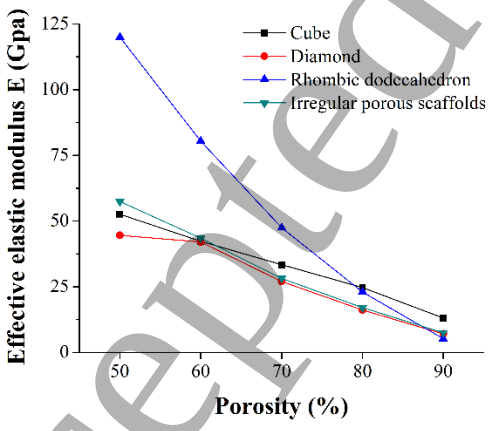

Figure 10. Relation between porosity and effective elastic modulus of four porous scaffolds.

In order to better compare the compressive strength of each model, the finite element model node average stress is introduced. This is because when the strain is 0.01, in the same porous

structure, the greater the average stress of all nodes in the compression test simulation, the stronger the ability of the model to resist deformation. That is, the compressive strength of the model is positively correlated with the average stress of all nodes in the model. Figure 11 shows that as the porosity increases, the average stress of the four porous structural finite element model nodes decreases to varying degrees, which indirectly indicates that the compressive strength of the four models is reduced to varying degrees with a strain of 0.01. The cube structure has the highest compressive strength, and with the increase of porosity, the compressive strength of the rhombic dodecahedron structure decreases the fastest, which is obviously more susceptible to the change of porosity.

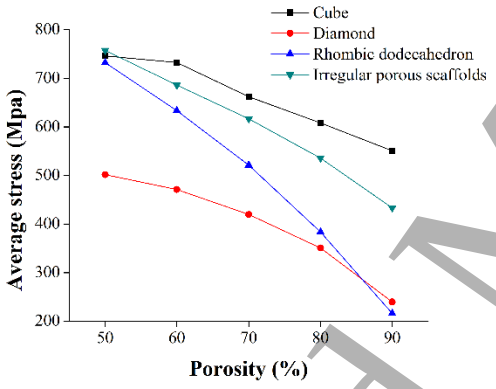

Figure 11. Relation between porosity and average stress of four porous scaffolds.

Figure 12 shows the trend of the maximum compressive stress of four porous structures under different porosity conditions. Except for the irregular porous structure showing a steady upward trend, the other three are fluctuations but the overall decline trend. The maximum compressive stress of the porous model is closely related to the structure of the model and the boundary conditions of the simulation. Under the same boundary conditions, from Fig. 13, the four porous structural stresses are mainly concentrated at the joints connected by the struts. Compared with the uniformity of the regular porous structure, in the irregular porous structure, there may be some relatively weak struts

and the stress is excessively concentrated at the joints, and the phenomena of stress concentration at the joints in the irregular porous scaffolds are more than others.

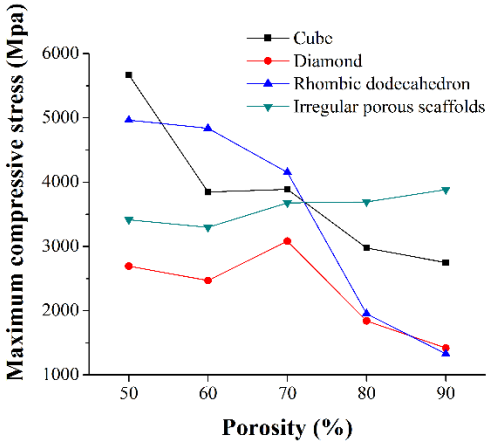

Figure 12. Relation between porosity and maximum compressive stress of four porous scaffolds.

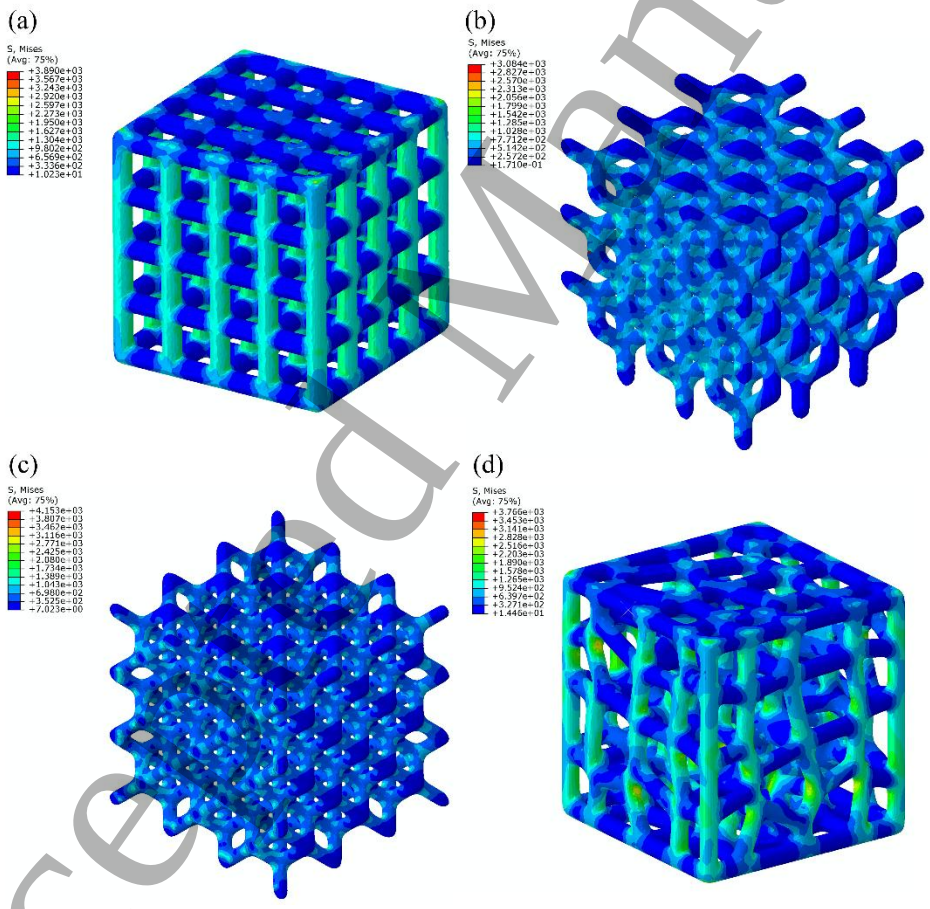

Figure 13. Von-Mises contour plots for different porous scaffolds with 70% porosity. (a) Cube scaffolds. (b) Diamond scaffolds. (c) Rhombic dodecahedron scaffolds. (d) Irregular porous scaffolds.

Basically, due to the interaction between the layers during compression, the mechanical response of typical cellular materials differs from the mechanical response of solid materials [29]. Many studies have distinguished the resulting patterns of cellular materials as stretch dominated and bending dominated deformations. Maxwell introduced an algebraic criterion with a frame of b struts and j frictionless joints, in three dimensions, the equivalent equation is

$$M = b - 3j + 6 \quad (6)$$

If M <0, the frame is a mechanism and locking joints cause struts to bend. Then, the deformation of equivalent foam is bending dominated. Instead, if $M \geqslant 0$, the frame is a structure and struts carry axial stresses. Whereas it causes struts to stretch, deformation mode is stretch dominated for equivalent foam [30].From Table 1, these four porous structures belong to the bending dominant deformation. An increase in Maxwell's value means that the average number of struts per joint increases, connectivity is higher, resulting in higher structure rigidity [31]. On the contrary, the smaller the Maxwell value is, the worse the rigidity is, and the porous structure is characterized by an elastic modulus that is much lower than that of the solid material model, thereby achieving the goal of matching the elastic modulus of bone tissue.

In fact, by reasonably adjusting the structural design parameters (strut diameter, unit distance, irregularity), the mechanical properties of the four porous structures can be better matched to the requirements of bone tissue engineering.

Table 1. Maxwell number for unit cell candidate lattice structures

Cell type	Cube	Diamond	Rhombic dodecahedron	Irregular porous scaffolds
Struts, b	300	432	864	688
Joints, j	125	276	388	346

Maxwell value, *M*	-69	-390	-294	-344

3.4 Anisotropy of the irregular porous scaffolds

Among these four porous structures, the irregular porous structure is most unique because of the irregularity. In theory, due to the randomness of the seed point arrangement, a number of irregular Voronoi cells are generated spatially. The structural anisotropy of the irregular porous structure is finally formed. In order to evaluate the anisotropy of irregular porous structures, we performed compression and permeability simulations on the irregular porous structures with different porosity gradients in x, y, and z directions.

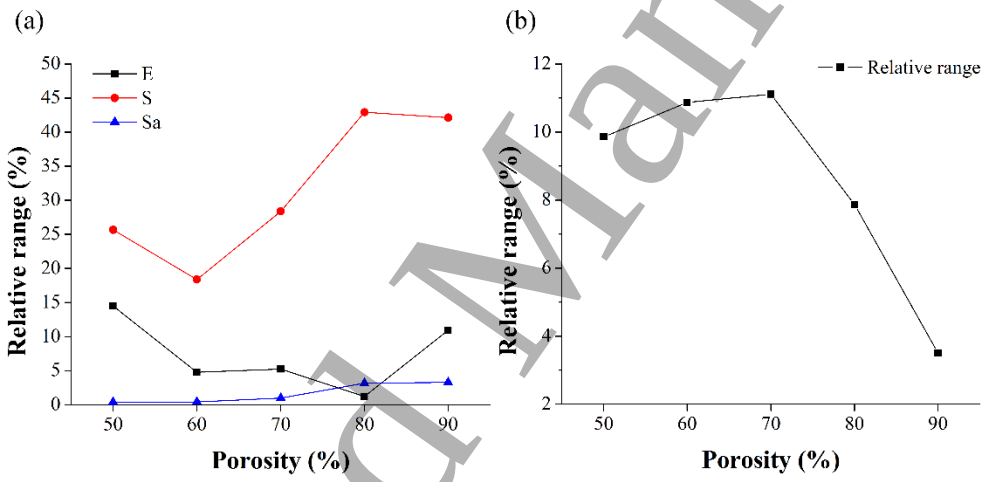

Figure 14. Relative range of different irregular porous. (a) Mechanical properties. (b) Permeability

On the one hand, it can be seen from Fig. 14(a) that as the porosity increases, the maximum compressive stress fluctuates within a large range of 18% to 43%. The relative range of the average stress at all nodes of the entire irregular porous structure increases from 0.41% to 3.3% with increasing porosity, the most important, the relative range of the effective elastic modulus fluctuates within 15%. On the other hand, as the porosity increases, the relative range of the permeability of the irregular porous structure undergoes a process of increasing first and then decreasing in the Fig.

14(b), the maximum and minimum values are 11.11% and 3.51%, respectively.

In general, the relative range of the results of compression and permeation simulation from the x, y, and z directions of the irregular porous structure is basically within a controllable range, especially the effective elastic modulus and permeability. The relative range of the index is within 15% and 12% respectively, which indicates that the influence of structural anisotropy on the effective elastic modulus and permeability is relatively limited. Previous studies using similar methods to construct irregular porous structures has also shown that the degree of anisotropy of irregular porous structures is low [18].

When the number of Voronoi cells of irregular porous structure increases, in view of the characteristics of randomly generating seed point Voronoi diagrams, each direction of irregular porous structures will be more balanced, and the anisotropy of effective elastic modulus and permeability will be gradually reduced.

4. Conclusion

In this study, we constructed four porous structures (cube, diamond, rhombic dodecahedron, irregular porous scaffold), which were tested though compression and permeability simulation under different porosity. The main findings are summarized as follows:

(1) As the porosity increases, the pore size and specific surface area of the four porous structures increase accordingly. In addition, different from the uniformity of the regular porous structure, the scattered distribution of through pores in the space and the scattered distribution of the pore size distribution undoubtedly make the irregular porous structure better imitate the human bone structure than the regular porous structure.

(2) The permeability of the four porous structures increased with the increase of porosity, and the structural properties (porosity, pore size, specific surface area) showed a positive correlation with permeability. Among them, the irregular porous structure has the largest coverage of permeability. ($0.71\text{-}23.05\text{x } 10^{-8}\text{m}^2$).

Different from the uniformity of the velocity contour in the regular flow structure, the special structural characteristics of the irregular porous structure cause the permeability non-uniformity, making the irregular porous structure similar to human bone, ensuring the transport of oxygen and nutrients, also conducive to cell adhesion and proliferation.

(3) As the porosity increases, the compressive strength and effective elastic modulus of the four porous structures generally decreases. When the porosity is 70% or higher, the elastic modulus is in the range of the elastic modulus of the human cortical bone (3-30 Gpa); For the four porous structures, the maximum compressive stress is mainly concentrated at the joint of the struts, and the fragile struts are more likely to occur in the irregular porous structure, resulting in a larger stress concentration.

(4) The effective elastic modulus and permeability were measured by the irregular porous structure with five different porosity in the three directions of x, y and z, the maximum relative range of effective elastic modulus and permeability is 14.5% and 11.11%, respectively, which indicates the effective elastic modulus and permeability show relatively limited anisotropy under the condition of random distribution of Voronoi diagram.

In summary, at 80% porosity, the effective elastic modulus and permeability of the four porous structures can basically meet the requirements of the implant. Structural characteristic of irregular porous structures similarly to human bones, as well as relatively limited anisotropy, showing

superior development application potential compared to regular porous structures.

Acknowledgements

The work was financially supported by the Advanced Research Project of Army Equipment Development (301020803), the Key Research and Development Program of Jiangsu (BE 2015161) , the Jiangsu Provincial Research Foundation for Basic Research, China (BK 20161476), the Science and Technology Planning Project of Jiangsu Province of China (BE 2015029) and the Science and Technology Support Program of Jiangsu (BE 2016010-3), The Nanjing University of Aeronautics and Astronautics major project cultivation plan(NP2017414),The Nanjing University of Aeronautics and Astronautics Youth Technology Innovation Fund (NT2018016).

Reference

[1]. Hedayati R, Sadighi M, Mohammadi-Aghdam M, Hosseini-Toudeshky H 2018 *J.Biomed. Mater. Res. Part B*. **106** 386-398

[2]. Borleffs MS 2012 Finite Element Modeling to Predict Bulk Mechanical Properties of 3D Printed Metal Foams. Delft University of Technology. Delft, the Netherlands

[3]. Sundfeldt M, Carlsson LV, Johansson CB, Thomsen P, Gretzer C 2006 *Acta orthop*. **77** 177–197

[4]. Karageorgiou V, Kaplan D 2005 *Biomaterials*. **26** 5474-5491

[5]. Hollister SJ 2009 *Adv.Mater*. **21** 3330-3342

[6]. Langer RS, Vacanti JP 1999 *Sci. Am*. **280** 86-89

[7]. Langer R, Vacanti JP 1993 *Science*. **260** 920-926

[8]. Cima, LG, Vacanti JP, Vacanti C, Ingber D, Mooney D, Langer R 1991 *J. Biomech. Eng*. **113**

143-151

[9].Langer R, Cima LG, Tamada JA, Wintermantel E, 1990 *Biomaterials*. **11** 738-745

[10]. Gibson, LJ. & Ashby MF. Cellular solids, structure and properties, 2nd edn. Cambridge, UK: Cambridge University Press.1997

[11]. Kadkhodapour J, Montazerian H, Darabi AC, Anaraki AP, Ahmadi SM, Zadpoor AA, Schmauder S 2015 *J. Mech. Behav. Biomed. Mater.* **50** 180–191

[12]. Ahmadi SM, Campoli G, Yavari SA, Sajadi B, Wauthle R, Schrooten J, Weinans H, Zadpoor AA. 2014 *J Mech Behav Biomed Mater.* **34** 106–115

[13]. Campoli G, Borleffs MS, Yavari SA, Wauthle R, Weinans H, Zad-poor AA 2013 *Mater Des.* **49** 957–965

[14]. Horn TJ, Harrysson OLA, Marcellin-Little DJ, West HA, Lascelles BDX, Aman R, 2014 *Addit. Manuf*. **1–4** 2–11

[15]. Cao XF, Duan SY, Liang J, Wen WB, Fang DN 2018 *Int. J. Mech. Sci*. **145** 53-63

[16]. Sun JF, Yang YQ, Wang D 2012 *Adv. Mech. Eng*. **9** 742-760

[17]. Mullen L, Stamp RC, Brooks WK, Jones E, Sutcliffe CJ, 2009 *J Biomed Mater ResB Appl Biomater*. **89** 325–334

[18]. Fantini M, Curto M 2018 *Int. J. Interact. Des. Manuf*. **12** 585–596.

[19]. Wang, G.J, Shen, L.D, Zhao J.F, Liang, H.X, Xie, D.Q, Tian Z.J, Wang, C.J 2018 *ACS Biomater. Sci. Eng*. **4** 719–727

[20]. Olivares AL, Marsal E, Planell, JA, Lacroix D 2009 *Biomaterials*. **30** 6142–6149

[21]. Kadkhodapour J, Montazerian H, Darabi AC, Zargarian A, Schmauder S 2017 *J. Mech. Behav. Biomed. Mater.***70** 28-42

[22]. Stamboulis, AG, Boccaccini, AR, Hench, LL 2002 *Adv. Eng. Mater.* **4** 105-109

[23]. Gomez S, Vlad MD, Lopez J, Fernandez E 2016 *Acta Biomater.* **42** 341-350

[24]. Syahrom A, Kadir MRA, Kadir, Abdullah J, Ochsner A 2013 *Med. Eng. Phys.* **35** 792–799

[25]. Widmer RP, Ferguson SJ, 2013 *Proc. Inst. Mech. Eng. H* **227** 617–628

[26]. Nauman EA, Fong KE, Keaveny TM 1999 *Ann. Biomed. Eng.* **27** 517–524

[27]. Liang HX, Yang, YW, Xie DQ, Li L, Mao N, Wang CJ, Tian ZJ, Jiang Q, Shen LD 2019 *J. Mater. Sci. Technol.* **35** 1284-1297

[28]. Wang, X.J, Xu, S.Q, Zhou, S.W, Xu, W, Leary, M, Choong, P, Qian, M, Brandt, M, Xi e, Y.M 2016 *Biomaterials.* **82** 127-141

[29]. Kadkhodapour J, Montazerian H, Raeisi S, 2014 *Mater. Sci. Eng. C-Mater. Biol. App l.* **43** 587-597

[30]. Ashby MF, 2006 *Philos. Trans. R. Soc. A.* **364** 15–30

[31]. Mazur M, Leary M, Sun SJ, Vcelka M, Shidid D, Brandt M 2016 *Int J Adv Manuf Technol.* **84** 1391–141